

An Optimal Frequency Control Method of Asynchronous Power Grid Considering Multi-HVDC
Emergency Power Support

Original

An Optimal Frequency Control Method of Asynchronous Power Grid Considering Multi-HVDC Emergency Power Support
/ Hu, Y; Wang, Xr; Huang, T; Lei, X; Wang, T. - In: IEEE ACCESS. - ISSN 2169-3536. - 10:(2022), pp. 78011-78021.
[10.1109/ACCESS.2022.3192569]

Availability:

This version is available at: 11583/2977277 since: 2023-03-21T14:39:06Z

Publisher:

IEEE-INST ELECTRICAL ELECTRONICS ENGINEERS INC

Published

DOI:10.1109/ACCESS.2022.3192569

Terms of use:

This article is made available under terms and conditions as specified in the corresponding bibliographic description in the repository

Publisher copyright

(Article begins on next page)

Received 21 June 2022, accepted 11 July 2022, date of publication 20 July 2022, date of current version 28 July 2022.

Digital Object Identifier 10.1109/ACCESS.2022.3192569

RESEARCH ARTICLE

An Optimal Frequency Control Method of Asynchronous Power Grid Considering Multi-HVDC Emergency Power Support

YI HU¹, XIAORU WANG², (Senior Member, IEEE), TAO HUANG³, (Member, IEEE),
XIA LEI¹, (Member, IEEE), AND TAO WANG¹¹School of Electrical Engineering and Electronic Information, Xihua University, Chengdu 610039, China²School of Electrical Engineering, Southwest Jiaotong University, Chengdu 611756, China³Department Ingegneria Elettrica, Politecnico Di Torino, 10129 Turin, Italy

Corresponding author: Yi Hu (huangganghui@163.com)

This work was supported in part by the Key Research and Development Projects in Sichuan Province, China, under Grant 2017GZ0054; and in part by the Technology Projects of State Grid Corporation of China under Grant SGTYHT/15-JS-191.

ABSTRACT Emergency DC power support has become an effective frequency stability control approach. For the asynchronous power grid with multi-HVDC links, this paper proposes an optimal control based on wide-area measurements (WAMS). The prominent advantage of this control is to improve the frequency stability of the disturbed grid while taking into account the influence on power flow, node voltage and other grid frequency fluctuations. In order to evaluate the post-disturbance frequency stability, a steady-state frequency prediction model based on WAMS data is first proposed, which can reflect the correspondence between post-disturbance steady-state frequency and the DC power support amount. In order to obtain the optimal control strategy, an optimization model is established to formulate the proposed control problem. The optimization objective of the model is to minimize the frequency deviation of interconnected power grids, and the constraints are to restore steady-state frequency to target value and ensure the security of line power flow and node voltage. The final control strategy is obtained by solving the optimization model. Simulations of the modified IEEE 50-generator system are performed to validate the accuracy of the proposed frequency prediction model and the effectiveness of the proposed frequency stability control.

INDEX TERMS Asynchronous power grid with multi-HVDC links, WAMS, frequency prediction, emergency DC power support, optimal frequency control.

I. INTRODUCTION

High voltage direct current (HVDC) transmission has been widely used because of its mature technology, large transmission capacity and strong controllable ability [1], [2]. It allows the frequencies and phase angles of interconnected AC power grids to operate independently, which has led to the emergence of more and more asynchronous power grids. For instance, as a part of China Southern Power Grid, Yunnan Power Grid is asynchronously interconnected with several neighboring provincial power grids by multi-HVDC links [3]. Moreover, because of the back-to-back voltage source converter based high voltage direct

current (VSC-HVDC) project constructed between Chongqing and Hubei, Southwest China Power Grid is asynchronously connected with Central China Power Grid and East China Power Grid [4]. These asynchronous power grids are isolated by HVDC links and lose the power mutual support with other power grids. In addition, with the large-scale connection of renewable energy source in the power grid, the inertia of the system is also gradually reduced. Consequently, the frequency stability problem of asynchronous power grids will become more serious if the disturbance of large power shortage occurs, such as the tripping of large-capacity generators and the channel blocking caused by large-capacity transmissions. Therefore, it is an important issue to enhance the frequency stability of the asynchronous power grids.

The associate editor coordinating the review of this manuscript and approving it for publication was Huiyan Zhang¹.

So far, extensive research on the frequency stability control has been carried out. The traditional under-frequency load shedding is the earliest way to control the frequency [5]–[7]. But for severe disturbance, frequency stability control requires higher timeliness, and traditional under-frequency load shedding may fail due to action delay. Therefore, the fast load shedding control has been proposed in [8]–[10]. Reference [8] used WAMS data to estimate the post-disturbance steady-state frequency, and a estimation model was established to calculate the amount of load shedding required to keep the frequency above target value. In Refs [9], [10], the linearization method was used to consider the network equations of the power grid into the estimation model, and the optimal load shedding amount through linear programming was obtained. These methods are effective for enhancing frequency stability, but large-capacity load removal is negative for the economic and reliable operation of the power grid.

HVDC link not only has strong controllability for transmission power, but also has less control cost, which will not affect the reliability of power supply. Therefore, the using of DC emergency power support to improve the post-disturbance frequency characteristics have been discussed in many studies, such as Refs. [11]–[15]. However, most of these studies only focus on the FLC control or additional frequency control of single HVDC link, and a few consider the coordinated frequency control between multiple HVDC links. Refs. [16]–[19] consider a power system composed of several asynchronously AC grids by multi-HVDC links. Once a disturbance occurs in one of the grids, the distributed frequency control was proposed to make the frequency deviations of all grids stay close to each other. In Refs. [20]–[22], the primary frequency control was addressed via both offshore wind power plants and the other AC grids. It proposed a coordinated frequency controller for mainland AC grid considering the reserve of wind power plants and power support of the MT-HVDC transmission system. This controller can maintain the frequencies of the disturbed AC grids close to the nominal value.

The main work of these studies is to use multi DC power support to participate in the frequency control. They focus on the design of coordination controllers, and the difficulty lies in the setting and calculation of control parameters. Since the parameters have great impacts on control results, the portability of the proposed controllers is greatly reduced. Moreover, these controllers do not take into account the impact of frequency control on power flow and node voltage. Therefore [23] began to discuss the frequency coordinated control from the perspective of frequency prediction and control quantity calculation, which bypassed the design of coordinated controllers. However, the proposed frequency response prediction model is too simple to accurately reflect the frequency characteristics after disturbances, resulting in a low control accuracy.

To address the aforementioned issues, this paper proposes a new frequency stability coordinated control strategy for the asynchronous power grid with multi-HVDC links. Firstly, a steady-state frequency prediction model based on WAMS data is constructed. Then, based on the model, an optimization model of frequency stability coordinated control is established according to the frequency control target. Finally, the optimal coordinated control strategy is obtained by solving the optimization model. The proposed control method has the following salient characteristics:

- The proposed method constructs a fast steady-state frequency prediction model based on the WAMS data before and after disturbance. The prediction accuracy of the model is high because that it comprehensively takes into account the effects of the generator primary frequency control, the load frequency variation effect, the system network loss and different HVDC control characteristics on frequency response characteristics in detail. Moreover, the calculation accuracy of control variables are also high because they are obtained based on the established prediction model.
- The coordination mechanism of our control method is more reasonable and comprehensive because it not only considers the accurate realization of the control targets, but also takes into account the influence of the control strategy on power flows, node voltages and the frequency deviation of each HVDC interconnected power grids.

The remainder of this paper is organized as follows. Section II proposes the post-disturbance steady-state frequency prediction model. The optimal frequency control considering multi-HVDC emergency power support is studied in Section III. Following, experiment results on IEEE 50-generator system with four HVDC links are provided in Section IV. Finally, conclusions are drawn in Section V.

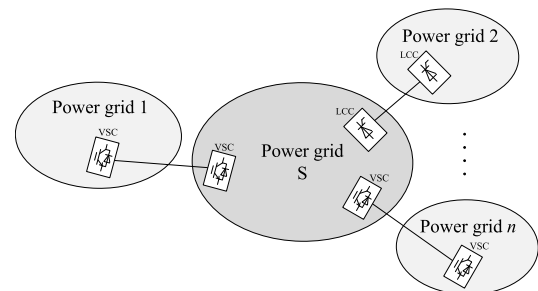


FIGURE 1. A asynchronous power grid with multi-HVDC links.

II. POST-DISTURBANCE STEADY-STATE FREQUENCY PRE-DICTION MODEL

The asynchronous power grid we considered is marked as S, who is connected asynchronously with other AC power grids by multi-HVDC links, as shown in Fig. 1. The HVDC

lines include both line commutated converter high voltage direct currents (LCC-HVDCs) and voltage sourced converter high voltage direct currents (VSC-HVDCs). In this paper, the emergency DC power support provided by the HVDC links is employed to ensure the frequency stability of power grid S.

Frequency prediction is a critical step before the start-up of frequency control. Consequently, a post-disturbance steady-state frequency prediction model based on WAMS data is firstly established in this section. The model is composed of the generator power equation, load power equation, HVDC transmission power equation and power grid network equation, which are described as follows.

A. POWER EQUATIONS OF GENERATORS AND LOADS

Ignoring mechanical damping, the swing equation for the nodes of generators can be presented as follows:

$$\begin{cases} \frac{d\delta}{dt} = \omega - 1 \\ H \frac{d\omega}{dt} = P_m - P_e = P_a \end{cases} \quad (1)$$

where δ is the power angle of generators; ω is the angular frequency; H is the inertia time constant; P_e , P_m and P_a are electromagnetic, mechanical and accelerating, respectively [24].

Because of droop characteristics of the primary frequency regulation of generators, the power increment equation of the i -th generator node can be expressed as:

$$\Delta P_{Gi} = P_{ei(\infty)} - P_{ei(0^+)} = -K_{Gi}\Delta\omega + P_{ai(0^+)} \quad (2)$$

where 0^+ and ∞ represent the instant after disturbance and the post-disturbance steady-state, respectively; P_{Gi} is the power injected into the grid of generator node; K_{Gi} is frequency regulation coefficient; $\Delta\omega$ is the increment of system inertia centre frequency [22].

If a generator is fully loaded, its governor cannot participate in the mechanical power regulation. When the i -th generator reaches its maximum active power output $P_{\max i}$, the corresponding frequency regulation coefficient will satisfy $K_{Gi} = 0$. In this case, Equation (2) is amended as:

$$\Delta P_{Gi} = (P_{\max i} - P_{mi(0^+)}) + P_{ai(0^+)} = \Delta P_{\max i} + P_{ai(0^+)} \quad (3)$$

For load nodes, the static load model with voltage and frequency dependence is considered as follows:

$$\begin{cases} P_l = P_{l0}(\alpha_p + \beta_p V_L + \gamma_p V_L^2)(1 + K_p \Delta\omega^*) \\ Q_l = Q_{l0}(\alpha_q + \beta_q V_L + \gamma_q V_L^2)(1 + K_q \Delta\omega^*) \end{cases} \quad (4)$$

where P_l and Q_l are the consumed active and reactive power of the load, respectively; P_{l0} and Q_{l0} are the consumed power at rated voltage and frequency, respectively; K_p and K_q represent the frequency variable factor of the active and reactive power, respectively; $\Delta\omega^*$ is the deviation between the actual and rating frequency of the load; α_p , β_p and γ_p represent the proportion of the constant power, constant current and

constant impedance for active loads while α_q , β_q and γ_q are the ones for reactive loads, respectively, who satisfy with $\alpha_p + \beta_p + \gamma_p = 1$ and $\alpha_q + \beta_q + \gamma_q = 1$. In this paper, we take $\alpha_p = \beta_q = \alpha_q = \beta_p = 0.1$ and $\gamma_p = \gamma_q = 0.8$.

From the instant after disturbance to the post-disturbance steady-state, the power increment equation of the i -th load node can be linearized as:

$$\begin{cases} \Delta P_{Li} = -(P_{li(\infty)} - P_{li(0^+)}) = -\frac{\partial P_{li}}{\partial \omega} \Delta\omega - \frac{\partial P_{li}}{\partial V_{li}/V_{li}} \frac{\Delta V_{li}}{V_{li}} \\ \Delta Q_{Li} = -(Q_{li(\infty)} - Q_{li(0^+)}) = -\frac{\partial Q_{li}}{\partial \omega} \Delta\omega - \frac{\partial Q_{li}}{\partial V_{li}/V_{li}} \frac{\Delta V_{li}}{V_{li}} \end{cases} \quad (5)$$

where P_{Li} and Q_{Li} are the active and reactive power injected into the load node, respectively; ΔV_{li} is the voltage increment.

B. POWER EQUATIONS OF LCC-HVDC AND VSC-HVDC

Since LCC-HVDC and VSC-HVDC adopt different control methods, they have different control characteristics. Consequently, their transmission power equations are also different, which are described in detail in this section.

1) LCC-HVDC

A sending out HVDC transmission system is taken as an example to describe the power equation of these nodes connected with LCC-HVDC, where the sending grid is the power grid S and the receiving grid is the interconnected power grid i . The schematic diagram is shown in Fig. 2.

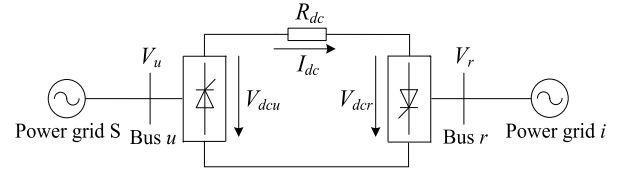


FIGURE 2. Schematic diagram of the LCC-HVDC transmission system.

According to the operating principle of LCC, there is a coupling relationship between the absorbed active and reactive power. The quasi-steady-state model of the sending LCC is given by [25]:

$$\begin{cases} V_{d0} = (3\sqrt{2}/\pi)V_u \\ V_{dcu} = V_{d0} \cos \alpha - (3X_c/\pi)I_{dc} \\ P_{dc} = V_{dcu}I_{dc} \\ Q_{dc} = P_{dc} \tan \varphi \\ \cos \varphi = V_{dcu}/V_{d0} \end{cases} \quad (6)$$

where V_{d0} is the open circuit DC voltage without phase control; V_u is the valve-side transformer voltage; X_c is the leakage reactance of transformer windings; I_{dc} , V_{dcu} , P_{dc} and Q_{dc} represent the DC current, voltage, absorbed active power and reactive power of the LCC, respectively; α is the trigger angle of LCC; φ is the power factor angle.

Considering the resistance R_{dc} of the DC line, the DC voltage V_{dcu} of the rectifier side can be obtained:

$$V_{dcu} = R_{dc}I_{dc} + V_{dcr} \quad (7)$$

In general, the active power regulation of LCC-HVDC system is realized by changing the DC current regulator. In this process, the inverter side DC voltage V_{dcr} is constant. Therefore, the nonlinear coupling relationship between the active and reactive power of the sending LCC station can be derived from Equations (6) and (7):

$$\begin{cases} Q_{dc}^2 = P_{dc}^2 \left(\frac{18V_u^2}{V_{dcr}^2 \pi^2} - 1 \right) \\ V_{dcr} = \frac{V_{dcr} + \sqrt{V_{dcr}^2 + 4R_{dc}P_{dc}}}{2} \end{cases} \quad (8)$$

When the power grid is in the steady-state, the node connected with LCC can be considered as a PQ node. Assume that the DC power regulation of the i -th LCC are ΔP_{dcAi} and ΔQ_{dcAi} . Considering the instant after disturbance and the post-disturbance steady-state, the power increment equations of the nodes connected with LCC-HVDC are:

$$\begin{cases} \Delta P_{DAi} = -\frac{\partial P_{li}}{\partial \omega} \Delta \omega - \frac{\partial P_{li}}{\partial V_{li}/V_{li}} \frac{\Delta V_{li}}{V_{li}} + \Delta P_{dcAi} \\ \Delta Q_{DAi} = -\frac{\partial Q_{li}}{\partial \omega} \Delta \omega - \frac{\partial Q_{li}}{\partial V_{li}/V_{li}} \frac{\Delta V_{li}}{V_{li}} + \Delta Q_{dcAi} \end{cases} \quad (9)$$

where ΔP_{dcAi} and ΔQ_{dcAi} satisfy the following coupling relationship.

$$\begin{cases} (Q_{dcAi}(0+) + \Delta Q_{dcAi})^2 = (P_{dcAi}(0+) + \Delta P_{dcAi})^2 \\ \left(\frac{18V_{Li}^2}{V_{dcr}^2 \pi^2} - 1 \right) \\ V_{dcr} = \frac{V_{dcr} + \sqrt{V_{dcr}^2 + 4R_{dc}(P_{dcAi}(0+) + \Delta P_{dcAi})}}{2} \end{cases} \quad (10)$$

2) VSC-HVDC

Different from LCC, VSC can control active power and reactive power independently, so its power equation has no coupling relationship.

Generally, VSC-HVDC has two common control modes [26], described as follows.

- Model I: Constant DC and AC voltage control are used on one side, and constant active power and AC voltage control are used on the other side;
- Model II: Constant DC voltage and reactive power control are used on one side, and constant active and reactive power control are used on the other side.

When in the control mode I, the actual active power and the AC voltage of the VSC are equal to the active power reference P_{dcref} and the AC voltage reference V_{acref} , respectively. Therefore, the node connected with VSC can be considered as a PV node in such a situation.

Assuming that the DC power regulation of the i -th VSC is ΔP_{dcBi} , the power increment equation of the node connected with VSC-HVDC is:

$$\Delta P_{DBi} = \Delta P_{dcBi} \quad (11)$$

When in the control mode II, the actual active and reactive power of the VSC are equal to the active power reference P_{dcref} and the reactive power reference Q_{dcref} . Therefore, the

node connected with VSC can be considered as a PQ node under this mode.

Define the active and reactive power regulation of the i -th VSC as ΔP_{dcCi} and ΔQ_{dcCi} , respectively. The power increment equation of the node connected with VSC-HVDC is:

$$\begin{cases} \Delta P_{DCi} = -\frac{\partial P_{li}}{\partial \omega} \Delta \omega - \frac{\partial P_{li}}{\partial V_{li}/V_{li}} \frac{\Delta V_{li}}{V_{li}} + \Delta P_{dcCi} \\ \Delta Q_{DCi} = -\frac{\partial Q_{li}}{\partial \omega} \Delta \omega - \frac{\partial Q_{li}}{\partial V_{li}/V_{li}} \frac{\Delta V_{li}}{V_{li}} + \Delta Q_{dcCi} \end{cases} \quad (12)$$

C. NETWORK EQUATION OF THE POWER SYSTEM

According to the power flow equation of power system, the injected power of any node in the grid can be expressed as:

$$P_i = V_i \sum_{j=1}^n V_j (G_{ij} \cos \theta_{ij} + B_{ij} \sin \theta_{ij}) \quad (13)$$

$$Q_i = V_i \sum_{j=1}^n V_j (G_{ij} \sin \theta_{ij} - B_{ij} \cos \theta_{ij}) \quad (14)$$

where P_i and Q_i are the injected active and reactive power, respectively; V_i is the node voltage amplitude; G_{ij} and B_{ij} are the mutual admittances; θ_{ij} is the voltage phase angle difference; n is the total number of the nodes.

Considering the instant after disturbance and the post-disturbance steady state, the injected power increment equation of all nodes is:

$$\begin{bmatrix} \Delta P \\ \Delta Q \end{bmatrix} = - \begin{bmatrix} H & N \\ J & L \end{bmatrix} \begin{bmatrix} \Delta \theta \\ \Delta V/V \end{bmatrix} \quad (15)$$

where $\Delta \theta$ and ΔV are the variations of voltage phase angle and amplitude, respectively; the expressions of H , N , J and L are the same with Newton-Raphson power flow method, which can be obtained by the voltage phase-angle and amplitude of the instant after disturbance.

D. POST-DISTURBANCE STEADY-STATE FREQUENCY PREDICTION MODEL

By substituting the power increment equations of the generator node (i.e., Equations (2) and (3)), the load node (i.e., Equation (5)) and the HVDC connected nodes (i.e., Equation (9), (11) and (12)) into Equation (15), the following correction equation can be obtained by derivation:

$$\begin{bmatrix} H_G & N_G & -K_G \\ H_L & N'_L & -\frac{\partial P_L}{\partial \omega} \\ H_D & N'_D & -\frac{\partial P_L}{\partial \omega} \\ J_L & L'_L & -\frac{\partial Q_L}{\partial \omega} \\ J_D & L'_D & -\frac{\partial Q_L}{\partial \omega} \end{bmatrix} \begin{bmatrix} \Delta \theta \\ \frac{\Delta V_L}{V_L} \\ \Delta \omega \end{bmatrix} = \begin{bmatrix} -P_{a(0+)} \\ 0 \\ 0 \\ 0 \\ 0 \end{bmatrix} - \begin{bmatrix} 0 \\ 0 \\ \Delta P_{dc} \\ 0 \\ \Delta Q_{dc} \end{bmatrix} \quad (16)$$

where $N'_L = N_L - \frac{\partial P_L}{\partial V_{li}/V_{li}}$; $N'_D = N_D - \frac{\partial P_L}{\partial V_{li}/V_{li}}$; $L'_L = L_L - \frac{\partial Q_L}{\partial V_{li}/V_{li}}$; $L'_D = L_D - \frac{\partial Q_L}{\partial V_{li}/V_{li}}$; ΔP_{dc} includes ΔP_{dca} , ΔP_{dcb} and ΔP_{dcc} while ΔQ_{dc} contains ΔQ_{dca} , and ΔQ_{dcb} ; the subscripts G and L represent generator node and load node,

respectively; the subscript D represents the node connected with HVDC link.

Due to the wide application of WAMS, the real-time various data before and after the disturbance can easily be obtained. The useful data include the generator electromagnetic power $P_{ei(0-)}$ in the instant before disturbance, the node voltage amplitude $V_{i(0+)}$, voltage phase-angle $\theta_{i(0+)}$, generator frequency $\omega_{i(0+)}$ and generator electromagnetic power $P_{ei(0+)}$ in the instant after disturbance. The Jacobian Matrix elements in Equation (16) can be calculated by $V_{i(0+)}$ and $\theta_{i(0+)}$. In the pre-disturbance steady-state, there is $P_{ei(0-)} = P_{mi(0-)}$. Since the mechanical power of the generator does not mutate after the disturbance occurs, there is $P_{mi(0+)} = P_{mi(0-)}$. According to Equation (1), $P_{ai(0+)}$ can be obtained by $P_{ei(0-)}$ and $P_{ei(0+)}$.

When the frequency stability control does not activate, that are $\Delta P_{dc} = 0$ and $\Delta Q_{dc} = 0$. If Equation (16) is expressed as $F(\Delta\theta, \Delta V_L, \Delta\omega, \Delta P_{dc}, \Delta Q_{dc}) = 0$, then the unknown quantities therein include only $\Delta\theta, \Delta V$ and $\Delta\omega$, that is $F(\Delta\theta, \Delta V_L, \Delta\omega) = 0$.

Accordingly, the post-disturbance steady-state frequency of the power grid can be quickly obtained by:

$$\begin{cases} F(\Delta\theta, \Delta V_L, \Delta\omega) = 0 \\ \omega(\infty) = \omega_{(0+)} + \Delta\omega \end{cases} \quad (17)$$

Equation (17) is the steady-state frequency prediction model of the power grid S with multi-HVDC links. This model establishes the mapping relationship between $\Delta\omega$ and ΔP_{dc} , which lays the foundation for the frequency stability control.

III. OPTIMAL FREQUENCY CONTROL CONSIDERING MULTI-HVDC EMERGENCY POWER SUPPORT

Assuming that $[\omega_{min}, \omega_{max}]$ is the accepted frequency security range of the power grid S. If the predicted $\omega(\infty)$ exceeds this range, the emergency frequency control will activate, which will use the power support of multi-HVDC links to enhance the power grid frequency stability.

Although the use of DC power support can restore the post-disturbance steady-state frequency of the power grid S to the target value, different power allocation of multi-HVDC links will have different effects on the power flow, node voltage and interconnected power grid frequency. Therefore, it is necessary to establish an optimization model for obtaining the optimal emergency power support for each HVDC link.

The desired post-disturbance steady-state frequency target is set as ω_{set} , which satisfies $\omega_{min} \leq \omega_{set} \leq \omega_{max}$. As a result, $\Delta\omega$ is a known quantity that can be obtained by:

$$\Delta\omega = \omega_{set} - \omega_{0+} \quad (18)$$

According to the frequency prediction model, considering that ΔP_{dc} and ΔQ_{dc} should be unknown quantities in the frequency stability control study, then the primary equality constraint equations of the optimization model

are obtained as:

$$\begin{cases} F(\Delta\theta, \Delta V_L, \Delta\omega, \Delta P_{dc}, \Delta Q_{dc}) = 0 \\ \Delta\omega = \omega_{set} - \omega_{0+} \end{cases} \quad (19)$$

When achieving the frequency stability control target of asynchronous power grid, it should also ensure that the frequency deviation of each interconnected power grid caused by DC power change meets the power quality requirements. Therefore, the constraint equations should include the security of steady-state frequency of the interconnected power grids.

The single machine equivalent model is used to describe the interconnected power grid:

$$\begin{cases} H_r \frac{d\omega_r}{dt} = P_{mr} - P_{er} = P_{ar} \\ \frac{d\delta_r}{dt} = \omega_r \end{cases} \quad (20)$$

where H_r is the total inertia time constant of the interconnected power grid; ω_r is the inertia centre frequency of the interconnected power grid; P_{mr} , P_{er} and P_{ar} are the total electromagnetic, mechanical and acceleration power of the interconnected power grid, respectively.

Assume that the active power change of the receiving end is ΔP_{dcr} . The acceleration power of the interconnected power grid is as follows:

$$P_{ar} = P_{ar0} - \Delta P_{ar} = \Delta P_{dcr} - K_{Sr} \Delta\omega_r \quad (21)$$

where K_{Sr} is the frequency regulation coefficient of the interconnected power grid.

Based on Equation (20) and (21), we can obtain that:

$$H_r \frac{d\omega_r}{dt} = \Delta P_{dcr} - K_{Sr}(\omega_r(\infty) - \omega_{r0}) \quad (22)$$

where ω_{r0} is the initial steady-state frequency of the interconnected power grid.

By solving Equation (22), the final steady-state frequency of the interconnected power grid can be obtained as follows:

$$\omega_r(\infty) = \omega_{r0} + \Delta P_{dcr} / K_{Sr} \quad (23)$$

Considering the power loss of the HVDC line, the relationship between ΔP_{dc} and ΔP_{dcr} is:

$$\Delta P_{dc} = \Delta P_{dcr} + I_{dc}^2 R_{dc} = \Delta P_{dcr} + \frac{(V_{dcu} - V_{dcr})^2}{R_{dc}} \quad (24)$$

For each HVDC link, the following relationship exists:

$$P_{dcr} = I_{dc} V_{dcr} = P_{dcu} - I_{dc}^2 R_{dc} \quad (25)$$

As a result of the HVDC control, a more specific relationship between ΔP_{dc} and ΔP_{dcr} can be obtained by Equation (8):

$$\begin{cases} \Delta P_{dcr} = \Delta P_{dc} - \frac{(V_{dcu} - V_{dcr})^2}{R_{dc}} \\ V_{dcu} = \frac{V_{dcr} + \sqrt{V_{dcr}^2 + 4R_{dc}(P_{dc(0)} + \Delta P_{dc})}}{2} \end{cases} \quad (26)$$

where $P_{dc(0)}$ is the initial active power transmitted by the sending-end of HVDC link.

The security range of frequency requirements for each interconnected power grid is set as $[\omega_{r\min i}, \omega_{r\max i}]$, and the inequality constraint equations for the i -th interconnected power grid can be obtained:

$$\begin{cases} \omega_{r\min i} - \omega_{0i} \leq \Delta\omega_{ri} \leq \omega_{r\max i} - \omega_{0i} \\ \Delta\omega_{ri} = \frac{\Delta P_{dcri}}{K_{Sri}} \\ \Delta P_{dcri} = \Delta P_{dci} - \frac{(\sqrt{V_{dcri}^2 + 4R_{dci}(P_{dci(0+)} + \Delta P_{dci})} - V_{dcr(i)})^2}{4R_{dci(i)}} \end{cases} \quad (27)$$

Although the frequency deviations of the interconnected power grids are constrained to meet the power quality requirements, this constraint is relatively loose. It should also be expected that the influence on frequency deviations of the interconnected power grids should be minimized. Therefore, the minimum sum of the squared frequency deviations of all interconnected power grids is taken as the optimized objective of the optimization model.

$$\min f(\Delta P_{dc}, \Delta Q_{dc}) = \sum_{i=1}^n |\Delta\omega_{ri}|^2 \quad (28)$$

where n is the number of interconnected power grids.

Since the overload capacity of the HVDC link is limited and different HVDC links have different overload capacities, the power regulation of the i -th HVDC should satisfy the inequality constraint equations:

$$\Delta P_{dci\min} \leq \Delta P_{dci} \leq \Delta P_{dci\max} \quad (29)$$

where $\Delta P_{dci\min}$ and $\Delta P_{dci\max}$ are the active power down-regulation and up-regulation limits of the HVDC link, including $\Delta P_{dcAi\min}$, $\Delta P_{dcBi\min}$, $\Delta P_{dcCi\min}$ and $\Delta P_{dcAi\max}$, $\Delta P_{dcBi\max}$, $\Delta P_{dcCi\max}$, respectively.

The emergency power support of multi-HVDC links change the power flow and node voltage while enhancing the frequency stability of the power grid S. Therefore, certain lines within the power grid S may be overloaded or even exceed the transmission capacity limit, and certain node voltages may also exceed the security range of power quality requirements. This makes it necessary to take the security of

the line transmission power and node voltage as a constraint equation, so that a more perfect optimal control optimization model can be established.

The steady-state of the power grid is taken into account after frequency stability control applied. The active power flow distribution from the i -th to the j -th node can be obtained as:

$$P_{lij} = V_{Li}^2 G_{ij} - V_{Li} V_{Lj} (G_{ij} \cos \theta_{ij} + B_{ij} \sin \theta_{ij}) \quad (30)$$

Set $P_{l(ij)\max}$ as the transmission power limit of the AC line from the i -th to the j -th node, and $[V_{L\min}, V_{L\max}]$ as the security range of the power grid node voltage, then the inequality constraint equations are as follows:

$$\begin{cases} V_{Li(\infty)}^2 G_{ij} - V_{Li(\infty)} V_{Lj(\infty)} (G_{ij} \cos \theta_{ij(\infty)} + B_{ij} \sin \theta_{ij(\infty)}) \\ < P_{l(ij)\max} \\ V_{L\min} \leq V_{Li(\infty)} \leq V_{L\max} \end{cases} \quad (31)$$

In summary, the optimization model for optimal control established in this paper can be described as (32), shown at the bottom of the page. By solving the nonlinear optimization model Equation (32), the optimal emergency power support of each HVDC link can be obtained.

IV. SIMULATION VERIFICATION

A. SIMULATION SYSTEM

An interconnected power system is employed to verify the correctness and effectiveness of the proposed method, where the modified IEEE 50-generator system is used to simulate as the power grid S and four HVDC links are used to interconnect with other asynchronous power grids. The main configuration of the modified IEEE 50-generator system is shown in Fig. 3, which consists of 50 generators and 95 loads. The system includes 5.02% of constant impedance load and 94.98% of constant power load.

In the interconnected system, the four HVDC links are respectively connected to Node 27, Node 59, Node 74 and Node 110 of the modified system. For the convenience of distinction, they are denoted as Link 1, Link 2, Link 3 and

$$\begin{aligned} \min \quad & f(\Delta P_{dc}, \Delta Q_{dc}) = \sum_{i=1}^n |\Delta\omega_{ri}|^2 \\ \text{s.t.} \quad & \begin{cases} F(\Delta\theta, \Delta V_L, \Delta\omega, \Delta P_{dc}, \Delta Q_{dc}) = 0 \\ \Delta\omega = \omega_{set} - \omega_{0+} \\ \omega_{r\min i} - \omega_{0i} \leq \Delta\omega_{ri} \leq \omega_{r\max i} - \omega_{0i} \\ \Delta\omega_{ri} = \frac{\Delta P_{dcri}}{K_{Sri}} \\ \Delta P_{dcri} = \Delta P_{dci} - \frac{(\sqrt{V_{dcri}^2 + 4R_{dci}(P_{dci(0+)} + \Delta P_{dci})} - V_{dcr(i)})^2}{4R_{dci(i)}} \\ \Delta P_{dci\min} \leq \Delta P_{dci} \leq \Delta P_{dci\max} \\ V_{Li(\infty)}^2 G_{ij} - V_{Li(\infty)} V_{Lj(\infty)} (G_{ij} \cos \theta_{ij(\infty)} + B_{ij} \sin \theta_{ij(\infty)}) < P_{l(ij)\max} \\ V_{L\min} \leq V_{Li(\infty)} \leq V_{L\max} \end{cases} \end{aligned} \quad (32)$$

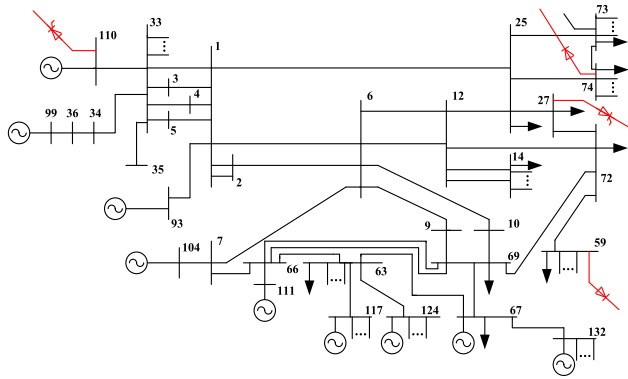


FIGURE 3. Modified 50-machine system.

Link 4, respectively. Among them, Link 2 and Link 3 are the LCC-HVDC links that employ constant power control to the rectifier and constant DC voltage control to the inverter, Link 1 and Link 4 are connected with two VSC-HVDC links that adopt control modes II and I, respectively. The basic parameters of each HVDC link are shown in Table 1.

TABLE 1. Basic parameters of HVDC links.

Parameters	Link 1 (Grid 1)	Link 2 (Grid 2)	Link 3 (Grid 3)	Link 4 (Grid 4)
$P_{dc(0)}$ /(MW)	1500	1600	1600	1500
ΔP_{dcmax} /(MW)	1000	1000	1000	1000
ΔP_{dcmin} /(MW)	-300	-300	-300	-300
V_{dcr} /(kV)	500	800	800	500
R_{dc} /(Ω)	1	1.5	1.5	1
K_{Sr}	2100	2400	1800	1500

System operating conditions: at $t = 0$ s, a three-phase short circuit fault occurs in line 1-25; at $t = 0.15$ s, the fault line is cut off; generator 104 is cut off at $t = 0.18$ s to prevent the system from transient instability. The total simulation time is 50s.

In this section, the proposed steady-state frequency prediction model and the optimal frequency stability control algorithm are realized by MATLAB. In addition, the PSS/E was used to perform time-domain simulation on the modified system. The time-domain simulation data obtained before and after the disturbance is treated as the WAMS data. Therefore, the time-domain simulation data before and after $t = 0.18$ s are used as the data of the pre-disturbance 0^- and post-disturbance 0^+ required by the algorithms respectively. Finally, the time-domain simulation results of PSS/E are used to verify the frequency prediction result and the optimal control effect.

B. CASE STUDY

1) CASE 1: VERIFICATION OF STEADY-STATE FREQUENCY PREDICTION MODEL

The traditional power system frequency prediction usually adopts single machine equivalent model, among which low-order system frequency response (SFR) model is the most

TABLE 2. Comparative analysis of prediction accuracy between SSFP model and SFR model.

Descripti on	Prediction /(Hz)	PSS/E /(Hz)	Absolute error/(Hz)	Relative error/%
SSFP	58.209	58.231	0.022	0.038
SFR	58.160	58.231	0.071	0.122

commonly used. In order to verify the accuracy of the proposed steady-state frequency prediction (SSFP) model, the calculation result of the SFR model and the SSFP model were compared with the PSSE simulation result. According to the set operating conditions of the system, the post-disturbance steady-state frequency obtained by PSS/E is 58.231Hz. Therefore, the prediction error analysis of the two models is shown in Table 2.

Table 2 shows the advantages of the proposed SSFP model over the traditional SFR model. Since the SSFP model can take into account the frequency-varying power of the load, the HVDC link and the network loss during the disturbance, the $\omega_{(\infty)}$ calculated by the SSFP model is closer to the actual simulation result and the error is smaller. This indicates that the proposed frequency prediction model can more accurately establish the corresponding relationship between power disturbance and steady-state frequency, which lays the foundation for more accurate frequency stability control.

2) CASE 2: VERIFICATION OF OPTIMAL FREQUENCY STABILITY CONTROL

In this case, the accepted frequency security range of the power grid S is set as 59.5~60.5 Hz. According to Case 1, $\omega_{(\infty)}$ obtained by frequency prediction model is 58.231 Hz, which is obviously beyond the accepted range. Therefore, the proposed optimal control will be activated urgently, and the steady-state frequency control target is set to 59.5 Hz (ω_{set}).

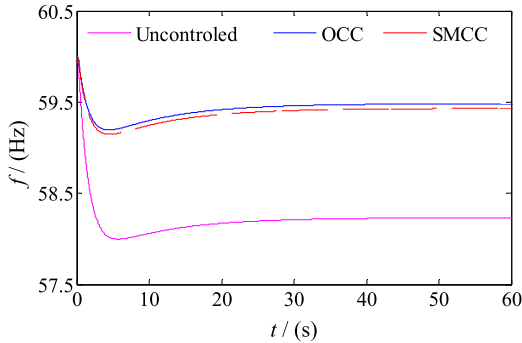
The key to obtain the optimal control scheme is to solve the optimization model. The optimization model established in this paper is a typical nonlinear optimization model because both the equality and inequality constraints contain nonlinear equations. To quickly obtain the optimal control scheme, the sequential quadratic programming (SQP) [27], [28] is employed to solve the established optimization model because it is an efficient nonlinear optimization solution method.

In order to verify the effectiveness of the proposed optimal coordinated control (labelled as OCC) and further illustrate its advantages, the same optimal control modelling idea is applied to the SFR model to establish traditional single-machine coordinated control (labelled as SMCC). According to $\omega_{set} = 59.5$ Hz, the emergency power support of each HVDC link obtained by the two optimal controls is shown in Table 3.

The PSS/E is used to simulate and verify the control schemes shown in Table 3, and the control is activated at $t = 0.2$ s. Finally, the inertia center frequency curve after disturbance under the two controls is obtained through

TABLE 3. Coordinated control scheme obtained by OCC and SMCC.

Descripti on	ΔP_{dc1} /(p.u.)	ΔP_{dc2} /(p.u.)	ΔP_{dc3} /(p.u.)	ΔP_{dc4} /(p.u.)
OCC	5.3811	2.5948	0.7794	1.1148
SMCC	2.3931	2.7350	2.0513	1.7094

**FIGURE 4.** Dynamic frequency curve of the power grid S.**TABLE 4.** Comparison of control accuracy between two control schemes.

Descripti on	Simulation /(Hz)	Target /(Hz)	Absolute error/(Hz)	Relative error/%
OCC	59.482	59.5	0.018	0.030
SMCC	59.431	59.5	0.069	0.116

simulation as shown in Fig. 4, and the steady-state frequency control effect is compared and verified in Table 4.

From Fig. 4 and Table 4, we can see that the SSFP model adopted by the proposed control has higher accuracy. The control error of the OCC is only about 26% of the SMCC, which shows that the proposed control method has obvious advantages over the traditional method. It can not only effectively enhance the frequency stability of the system, but also ensure that the post-disturbance steady-state frequency is accurately restored to ω_{set} .

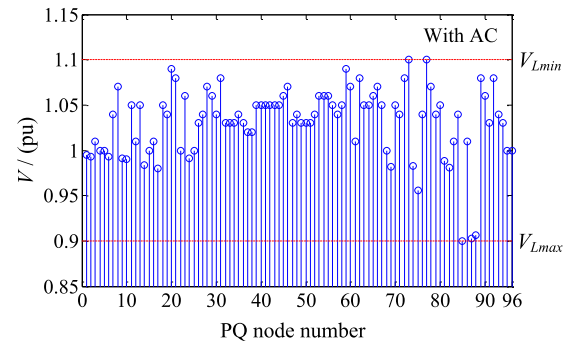
Moreover, table 4 and Fig. 4 also show that the post-disturbance steady-state frequency has been significantly improved, and can accurately reach the setting value after the frequency stability control applied. This finding verifies the accuracy and effectiveness of the proposed control.

3) CASE 3: NECESSITY VERIFICATION FOR THE CONSTRAINTS OF OPTIMAL FREQUENCY CONTROL

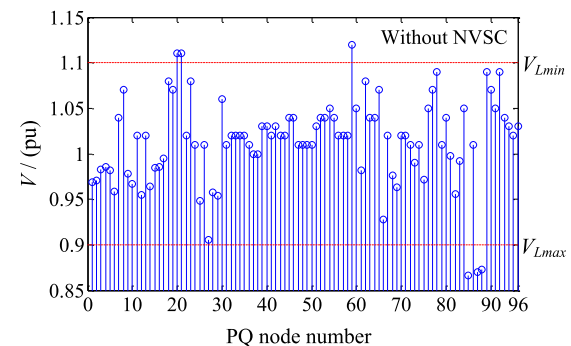
To illustrate the necessity of considering the line transmission power limit constraints (labelled as LTPLC), node voltage security constraints (labelled as NVSC) and interconnected grid frequency deviation constraints (labelled as FDC) in the proposed control, the optimization model is solved in the absence of corresponding constraints, and the different control schemes are obtained. The control effects of these schemes are compared with the optimal control scheme considering all constraints (labelled as AC), and the results are shown in Table 5 below.

TABLE 5. Comparison of optimization results and control effects in two cases.

Descripti on	ΔP_{dc1} /(p.u.)	ΔP_{dc2} /(p.u.)	ΔP_{dc3} /(p.u.)	ΔP_{dc4} /(p.u.)	PSS/E /(Hz)
With AC	5.3811	2.5948	0.7794	1.1148	59.482
Without LTPLC	5.3845	1.4287	2.8081	0	59.479
Without NVSC	4.0426	2.9535	1.4807	0.2989	59.477
Without FDC	7.1669	1.0252	0	1.0294	59.483



(a)



(b)

FIGURE 5. (a) PQ-node voltages with AC, and (b) PQ-node voltages without NVSC.

In Table 5, although there is a big difference in the amount of emergency power support of the same HVDC link in each control scheme, it can be seen from the steady-state frequency control effect that all the control schemes can restore the post-disturbance steady-state frequency to near the target value with small errors. Therefore, the necessity of each constraint cannot be determined from the frequency control target alone, and more control results of other aspects need to be presented.

Based on the PSSE time-domain simulation, the control results of the power grid after the implementation of the control schemes can be obtained. Firstly, after the implementation of the optimal control scheme with all constraints and the control scheme without LTPLC, the active power flow distribution of typical heavy-load lines is counted, and the remaining transmission power margins are calculated separately. The comparison results are shown in Table 6.

TABLE 6. Power distribution of partial heavy load lines.

Line No.	Transmission power limit/(MW)	With AC		Without LTPLC	
		Actual power/(MW)	Power margin/(MW)	Actual power/(MW)	Power margin/(MW)
1~93	124	109.767	14.233	105.231	18.769
6~7	181	185.868	-4.868	177.327	3.673
6~9	187	183.323	3.677	180.240	6.760
6~10	187	188.846	-1.846	180.241	6.759
6~12	195	195.923	-0.923	185.328	9.672
12~13	131	126.245	4.755	126.007	4.993
12~14	132	135.883	-3.883	127.005	4.995
12~25	138	138.247	-0.247	136.337	1.663
12~72	130	135.021	-5.021	127.266	2.734
33~34	164	161.337	2.663	157.804	6.196
33~35	165	162.007	2.993	158.407	6.593
33~37	165	165.562	-0.562	161.539	3.461
33~38	165	165.143	-0.143	161.564	3.436
33~39	165	163.994	1.006	160.895	4.105
33~40	165	164.984	0.016	160.895	4.105
33~49	165	164.979	0.021	161.991	3.009
33~50	165	164.979	0.021	161.914	3.086
33~110	194	166.658	27.342	167.730	26.270
34~36	124	121.224	2.776	119.425	4.575

Table 6 shows that for the control scheme without LTPLC, the transmission power of lines 6~7, 6~10, 6~12, 12~14, 12~25, 12~72, 33~37 and 33~38 would exceed the capacity limit. This comparison result demonstrates the necessity of using the line transmission power limit as a constraint for optimal frequency control.

Secondly, the node voltage simulation results after the implementation of the optimal control scheme and the control scheme without NVSC are compared in Fig. 5.

Fig. 5 shows that the voltage amplitudes of the nodes 20, 21, 59, 85, 87 and 88 are beyond the security range when the control scheme without NVSC is implemented. It shows that the node voltage security constraints have an important role in the proposed control.

Finally, the frequency deviation of the interconnected grids after the implementation of the optimal control scheme and the control scheme without FDC are compared in Table 7.

TABLE 7. Steady-state frequency deviation of the interconnected power grids.

Descripti on	$\Delta\omega_1$ /(Hz)	$\Delta\omega_2$ /(Hz)	$\Delta\omega_3$ /(Hz)	$\Delta\omega_4$ /(Hz)
With AC	0.200	0.093	0.047	0.077
Without FDC	0.254	0.037	0	0.058

The security frequency deviation range of interconnected power grids is set as 59.8~60.2 Hz in this case. It can be seen from Table 7 that the steady-state frequency deviations of interconnected power grid 1 exceeds the security range when there is no FDC. This case verifies the importance of the frequency deviation constraint of the interconnected grids in the optimal control.

4) CASE 4: ANALYSIS OF THE RELATIONSHIP BETWEEN K_{Sr} AND THE POWER SUPPORT OF EACH HVDC LINKS

The value of K_{Sr} reflects the power support capacity of the interconnected power grid to participate in the frequency stability control. In the traditional control methods, the emergency power support of each HVDC link is usually allocated based on the value of K_{Sr} . In order to analyse the relationship between K_{Sr} and the power support amount of HVDC link, a series of optimization results for interconnected power grids with different K_{Sr} have been obtained from Table 8. The comparison results are shown in the groups 1-3 of Table 9. In addition, for the further comparison and analysis, the optimization results without any constraints are shown in Group 4 of Table 9.

TABLE 8. Grouping of interconnected power grids with different K_{Sr} .

Group No.	Grid 1	Grid 2	Grid 3	Grid 4
1	2100	2400	1800	1500
2	2400	1500	2100	1800
3	1500	2100	1800	2400
4	2100	2400	1800	1500

TABLE 9. Comparison of optimization results and PSS/E verification results of different groups.

Group No.	ΔP_{dc1} /(p.u.)	ΔP_{dc2} /(p.u.)	ΔP_{dc3} /(p.u.)	ΔP_{dc4} /(p.u.)	PSS/E/(Hz)
1	5.3811	2.5948	0.7794	1.1148	59.482
2	6	0	2.6392	1.1933	59.479
3	3.8462	0.7545	4.6154	1.4482	59.483
4	0.8273	7.6927	0	0	59.479

It can be seen from Table 8 and Table 9 that after considering the security constraints in the frequency stability control,

the emergency power support of each HVDC link is not positively related to K_{Sr} of the interconnected power grids. However, they are positively related when all the constraints are not considered. Therefore, it is unreasonable to allocate the power support of each HVDC link only based on the value of K_{Sr} , and the interconnected power grid with the strongest power regulation capability does not necessarily to play a leading role in the frequency control of power grid S.

V. CONCLUSION

For the power grid connected asynchronously with other power grids by multi-HVDC links, a post-disturbance steady-state frequency prediction model based on the WAMS is presented in this paper. Furthermore, considering that the predicted steady-state frequency exceeds the accepted security range, an optimal control method is proposed with multi-HVDC links participating in the frequency stability control in an optimally coordinated manner. To achieve such a control, this paper establishes a nonlinear optimization model. The objective function of this model is to minimize the sum of squares frequency deviations of the interconnected power grids. The constraint conditions of this model are: (a) ensuring the frequency of the power grid S to reach the specified value; (b) ensuring that the power flow and node voltage of the power grid S meet the security limit requirements; (c) ensuring that the frequency deviation of the interconnected grids meet the frequency quality requirements. The classical SQP algorithm is used to solve the optimization model, so that the optimal emergency power support for each HVDC link participating frequency stability control is quickly obtained. Case studies demonstrate the high accuracy of post-disturbance steady-state frequency prediction and advanced control performance.

REFERENCES

- [1] J. Wang, M. Huang, C. Fu, H. Li, S. Xu, and X. Li, "A new recovery strategy of HVDC system during AC faults," *IEEE Trans. Power Del.*, vol. 34, no. 2, pp. 486–495, Apr. 2019.
- [2] M. Wang, T. An, H. Ergun, Y. Lan, B. Andersen, M. Szechtman, W. Leterme, J. Beerten, and D. V. Hertem, "Review and outlook of HVDC grids as backbone of the transmission system," *CSEE J. Power Energy Syst.*, vol. 7, no. 4, pp. 797–810, Jul. 2021.
- [3] B. Zhou, H. Rao, W. Wu, T. Wang, C. Hong, D. Huang, W. Yao, X. Su, and T. Mao, "Principle and application of asynchronous operation of China southern power grid," *IEEE J. Emerg. Sel. Topics Power Electron.*, vol. 6, no. 3, pp. 1032–1040, Sep. 2018.
- [4] Y. Shu, G. Tang, and H. Pang, "A back-to-back VSC-HVDC system of Yu-E power transmission lines to improve cross-region capacity," *CSEE J. Power Energy Syst.*, vol. 6, no. 1, pp. 64–71, Mar. 2020.
- [5] T. Shekari, F. Aminifar, and M. Sanaye-Pasand, "An analytical adaptive load shedding scheme against severe combinational disturbances," *IEEE Trans. Power Syst.*, vol. 31, no. 5, pp. 4135–4143, Sep. 2016.
- [6] J. Hu, J. Cao, J. M. Guerrero, T. Yong, and J. Yu, "Improving frequency stability based on distributed control of multiple load aggregators," *IEEE Trans. Smart Grid*, vol. 8, no. 4, pp. 1553–1567, Jul. 2017.
- [7] C. Li, Y. Wu, Y. Sun, H. Zhang, Y. Liu, Y. Liu, and V. Terzija, "Continuous under-frequency load shedding scheme for power system adaptive frequency control," *IEEE Trans. Power Syst.*, vol. 35, no. 2, pp. 950–961, Mar. 2020.
- [8] M. Larsson, "An adaptive predictive approach to emergency frequency control in electric power systems," in *Proc. 44th IEEE Conf. Decis. Control*, Seville, Spain, Dec. 2005, pp. 4434–4439.
- [9] W. Zhang, X. Wang, and G. Liao, "Automatic load shedding emergency control algorithm of power system based on wide-area measurement data," *Power Syst. Technol.*, vol. 33, no. 3, pp. 69–73, Feb. 2009.
- [10] Y. Hu, X. Wang, Y. Teng, and Y. Che, "Optimal load shedding scheme of AC/DC hybrid receiving end power grid after UHVDC blocking," *Power Syst. Autom.*, vol. 44, no. 22, pp. 98–106, Nov. 2018.
- [11] P. Kou, D. Liang, Z. Wu, Q. Ze, and L. Gao, "Frequency support from a DC-grid offshore wind farm connected through an HVDC link: A communication-free approach," *IEEE Trans. Energy Convers.*, vol. 33, no. 3, pp. 1297–1310, Sep. 2018.
- [12] H. Rao, W. Wu, T. Mao, B. Zhou, C. Hong, Y. Liu, and X. Wu, "Frequency control at the power sending side for HVDC asynchronous interconnections between Yunnan power grid and the rest of CSG," *CSEE J. Power Energy Syst.*, vol. 7, no. 1, pp. 105–113, Jan. 2020.
- [13] J. Lee, S. Jeong, H. Kim, Y. Yoo, S. Jung, M. Yoon, and G. Jang, "Analytical approach for fast frequency response control of VSC HVDC," *IEEE Access*, vol. 9, pp. 91303–91313, 2021.
- [14] D.-H. Kwon, Y.-J. Kim, and O. Gomis-Bellmunt, "Optimal DC voltage and current control of an LCC HVDC system to improve real-time frequency regulation in rectifier- and inverter-side grids," *IEEE Trans. Power Syst.*, vol. 35, no. 6, pp. 4539–4553, Nov. 2020.
- [15] G.-S. Lee, D.-H. Kwon, S.-I. Moon, and P.-I. Hwang, "A coordinated control strategy for LCC HVDC systems for frequency support with suppression of AC voltage fluctuations," *IEEE Trans. Power Syst.*, vol. 35, no. 4, pp. 2804–2815, Jul. 2020.
- [16] J. Dai, Y. Phulpin, A. Sarlette, and D. Ernst, "Coordinated primary frequency control among non-synchronous systems connected by a multi-terminal high-voltage direct current grid," *IET Gener., Transmiss. Distrib.*, vol. 6, no. 2, pp. 99–108, Feb. 2012.
- [17] N. R. Chaudhuri, R. Majumder, and B. Chaudhuri, "System frequency support through multi-terminal DC (MTDC) grids," *IEEE Trans. Power Syst.*, vol. 28, no. 1, pp. 347–356, Feb. 2013.
- [18] T. N. Pham, H. Trinh, and A. M. T. Oo, "Distributed control of HVDC links for primary frequency control of time-delay power systems," *IEEE Trans. Power Syst.*, vol. 34, no. 2, pp. 1301–1314, Mar. 2019.
- [19] H. Shadabi and I. Kamwa, "Dual adaptive nonlinear droop control of VSC-MTDC system for improved transient stability and provision of primary frequency support," *IEEE Access*, vol. 9, pp. 76806–76815, 2021.
- [20] F. D. Bianchi, J. L. Dominguez-Garcia, and T. K. Vrana, "Distributed frequency control with partial information using MT-HVDC grids and WPPs," *IEEE Syst. J.*, vol. 13, no. 2, pp. 1694–1701, Jun. 2019.
- [21] M. M. Kabsha and Z. H. Rather, "A new control scheme for fast frequency support from HVDC connected offshore wind farm in low-inertia system," *IEEE Trans. Sustain. Energy*, vol. 11, no. 3, pp. 1829–1837, Jul. 2020.
- [22] A. Bidafar, O. Saborío-Romano, J. N. Sakamuri, N. A. Cutululis, V. Akhmatov, and P. E. Sørensen, "On feasibility of autonomous frequency-support provision from offshore HVDC grids," *IEEE Trans. Power Del.*, vol. 35, no. 6, pp. 2711–2721, Dec. 2020.
- [23] Y. Wen, C. Y. Chung, and X. Ye, "Enhancing frequency stability of asynchronous grids interconnected with HVDC links," *IEEE Trans. Power Syst.*, vol. 33, no. 2, pp. 1800–1810, Mar. 2018.
- [24] C. Fan, Y. Teng, J. Xie, and X. Wang, "Steady frequency prediction algorithm for power system with governor deadband," *Int. Trans. Elect. Energy Syst.*, vol. 28, no. 1, pp. 1–14, Oct. 2018.
- [25] M. Daryabak, S. Filizadeh, J. Jatskevich, A. Davoudi, M. Saeedifard, V. K. Sood, J. A. Martinez, D. Aliprantis, J. Cano, and A. Mehrizi-Sani, "Modeling of LCC-HVDC systems using dynamic phasors," *IEEE Trans. Power Del.*, vol. 29, no. 4, pp. 1989–1998, Aug. 2014.
- [26] L. Guan, X. Fan, Y. Liu, and Q. H. Wu, "Dual-mode control of AC/VSC-HVDC hybrid transmission systems with wind power integrated," *IEEE Trans. Power Del.*, vol. 30, no. 4, pp. 1686–1693, Aug. 2015.
- [27] X. Li, S. Ma, and Y. Wang, "Multi-population based ensemble mutation method for single objective bilevel optimization problem," *IEEE Access*, vol. 4, pp. 7262–7274, 2016.
- [28] H. Zhang, D. Yue, and X. Xie, "Robust optimization for dynamic economic dispatch under wind power uncertainty with different levels of uncertainty budget," *IEEE Access*, vol. 4, pp. 7633–7644, 2016.



YI HU was born in Chengdu, China, in 1990. He received the Ph.D. degree from the College of Electrical Engineering, Southwest Jiaotong University (SWJTU), China, in 2019. He has been a Lecturer with the School of Electrical Engineering and Electronic Information, Xihua University, since 2020. His research interest includes power system frequency stability analysis and control, especially for the AC/DC hybrid power grid.



XIA LEI (Member, IEEE) received the Ph.D. degree in electrical engineering from Sichuan University. She is currently a Professor with the School of Electrical Engineering and Electronic Information, Xihua University. Her research interests include the optimal operation of electrical systems with renewable energy and power markets.



XIAORU WANG (Senior Member, IEEE) received the Ph.D. degree from the School of Electrical Engineering, Southwest Jiaotong University, China, in 1998. She is currently a Full Professor with the School of Electrical Engineering, Southwest Jiaotong University. Her research interests include power system stability analysis and control, renewable energy, and intelligent power technology.



TAO HUANG (Member, IEEE) received the Ph.D. degree from the Politecnico di Torino, Turin, Italy. He is currently working as the Ph.D. Student Supervisor with the Department of Energy, Politecnico di Torino. His research interests include critical infrastructure protection, vulnerability detection and resilience enhancement, electricity markets, and smart grids.



TAO WANG received the Ph.D. degree in electrical engineering from the College of Electrical Engineering, Southwest Jiaotong University (SWJTU), China, in 2016. She is currently an Associate Professor with the School of Electrical Engineering and Electronic Information, Xihua University. Her research interests include the safe and stable operation of smart grid and energy internet.

...